Computational Study of Axial Fatigue for Peripheral Nitinol Stents

Alessio Meoli, Elena Dordoni, Lorenza Petrini, Francesco Migliavacca, Gabriele Dubini, and Giancarlo Pennati

(Submitted October 4, 2013; in revised form February 12, 2014; published online April 5, 2014)

1. Introduction

Among the different interventional techniques for the treatment of stenotic peripheral arteries to restore blood flow perfusion, the placement of self-expanding Nitinol stents, after pre-dilatation with an angioplasty balloon, has emerged as a standard endovascular procedure. Several clinical studies (Ref 1-6) reported high rates of technical success of the stenting procedure for the femoropopliteal region and higher vessel patency rates in the medium to a long-term follow-up than that obtained with balloon angioplasty alone. However, the long-term effectiveness of these devices is undermined by complications related to fatigue failure. In this region, hip and knee joint movements during gait produce quite large and cyclic deformations of the stented artery, such as axial compression and bending. These cyclic loads combined with the effects due to the arterial blood pressure may cause the fatigue fracture of the implanted stents. Fracture rates up to 50% have been reported in clinical studies (Ref 7-9) with a significant correlation between the incidences of stent fracture, the lesion length, and the number of implanted devices to treat a single long lesion. Although the number of fractured superficial femoral artery (SFA) stents was largely reduced using second-generation devices, remarkable differences still exist among different products. Reported fracture rates for commercially available self-expandable stents differ widely from 1.8 to 18% (Ref 10-12). Fatigue failure typically occurs in cases of very long lesions, which often require the use of two or more overlapping stents. Moreover, several authors (Ref 5, 7-9) observed that in case of overlapping stents, fracture often occurs in the region next to the overlapping portion. Even if stent fractures were reported also for coronary (Ref 13) and renal (Ref 14, 15) vascular districts, only few studies investigated this phenomenon and the causes of the observed failures have not yet been clarified. Hsiao et al. (Ref 16) investigated the effect of kidneys' movement due to respiration simulating in a cadaver model the implant of cobalt-chromium balloon expandable stents for two different clinical scenarios. They found that the degree of bending imposed to the devices by the renal artery movement depends on the simulated scenarios. In particular, in case of two overlapping stents, the longer stented segment was forced to conform to the bending curvature of the renal arteries and subjected to greater degree of bending than the single stent. They accounted for this effect in a fatigue computational analysis in a simplified way, hypothesizing that the overlapping section is relatively stiffer compared to the other two free ends. Therefore, the overlapping section of the stent was considered to be the fixed end with the non-overlapping section of the stent hanging free. As expected, they

Alessio Meoli, **Elena Dordoni**, **Francesco Migliavacca**, **Gabriele Dubini** and **Giancarlo Pennati**, Laboratory of Biological Structure Mechanics, Chemistry, Materials and Chemical Engineering Department "Giulio Natta", Politecnico di Milano, Piazza Leonardo da Vinci 32, 20133 Milan, Italy; and **Lorenza Petrini**, Department of Civil and Environmental Engineering, Politecnico di Milano, Milan, Italy. Contact e-mail: giancarlo.pennati@polimi.it.

found higher fracture risk associated with the overlapping stent configuration as a consequence of the higher degree of bending applied to device in this configuration.

In a recent study, Kapnisis et al. (Ref 17) explored the fatigue behavior of Nitinol coronary stents subjected to accelerated pulsatile fatigue testing in case of overlapping stents deployed in a natural rubber latex tube simulating the presence of a coronary artery. They found fretting wear and fatigue features on stent surfaces after exposure to cyclic loading similar to that arising in vivo from the systolic and diastolic blood pressure in the coronary circulation. Moreover, they found that biomechanical factors such as arterial curvature combined with stent overlapping enhance the incidence and degree of wear and fatigue fracture when compared to single stents in a straight tube configuration.

Regarding peripheral Nitinol stents, Smouse et al. (Ref 18) hypothesized that stent fractures were due to the fact that the overlapping portion has a greater stiffness than that of the individual stents, and as such tends to deform less in relation to the biomechanical forces acting in the femoropopliteal region. Therefore, in the stent portions adjacent to the overlapping region, a stress concentration leading to stent failure is generated. In this regard, finite element modeling represents an important analysis tool since it provides information on cyclic stress and strain fields throughout the stent, allowing the evaluation of the mechanical fatigue resistance of these devices.

In this study, to better understand the fatigue performance of Nitinol peripheral stents, a computational approach was adopted to investigate the effect of cyclic axial compression on their fatigue resistance, simulating different scenarios by means of the finite element method (FEM). To our knowledge, this is the first study that investigates the overlapping configuration for Nitinol peripheral stents when subjected to in vivo loading conditions typical for the SFA.

2. Materials and Methods

The fatigue behavior of self-expandable Nitinol stents was investigated by means of the FEM. For this purpose, a stent model (indicated as Stent M) resembling a commercial device from Invatec (Medtronic, Roncadelle, BS, Italy) was developed. Fatigue response of the device subjected to cyclic axial compression was investigated in different conditions: fully expanded stent, stent deployed in a tube, and two stents deployed in a tube with partial overlapping region. Numerical analyses were conducted using the commercial code ANSYS Mechanical APDL 13.0 (Ansys Inc., Canonsburg, PA, USA).

2.1 Stent Models

The 3D stent geometry was built starting from stereomicroscope images of real device. The Stent M has an open-cell design with peak-to-peak connection between each strut crown; the external diameter is equal to 8 mm. Concerning stents length, in case of a single device, 45.8 mm was used, while in case of overlapping devices two distinct stent models were created with a length of 28.4 mm each. Figure 1 shows the reconstructed stent geometry and the type of strut crown connections of the device.

Nitinol pseudoelastic material properties required for the ANSYS material model (Fig. 2) were based on previous experiments from our laboratory performed on samples made of typical biomedical Nitinol (Ref 19).

Stent models were discretized with highly regular hexahedral meshes using 8-node linear elements (SOLID185) with complete integration. A sensitivity test as in Meoli et al. (Ref 20) was performed ensuring that the proper number of elements was used. The best balance in terms of reasonable calculation time and solution accuracy was represented by the use of three elements either for thickness or width of the struts. Other computational studies (Ref 20-23) showed that the peaks of the stent struts are subjected to high deformation gradients. Hence, the number of elements in the longitudinal direction of the struts was increased, using a proper element size ratio, to obtain a finer mesh in those regions (Fig. 1c).

2.2 Fully Expanded Configuration

To investigate the fatigue behavior of peripheral stents subjected to cyclic axial compression, simulations were first performed in the fully expanded configuration. The load was applied through the imposition of displacement boundary conditions at the two stent sides (Ref 20). One end of the stent was kept fixed in all directions, while the other end was moved along the longitudinal axis of the stent to obtain a shortening of 5%. The applied loading was based on ranges measured in a cadaver model (Ref 24) and consistent with in vivo ranges of deformation present in the literature (Ref 25-27). The loading configuration was based on the configuration adopted by Müller-Hülsbeck et al. (Ref 28) in which different stents in the market were subjected to cyclic axial compression without considering the stent-vessel interaction. Figure 3a shows a scheme of the loading condition.

2.3 Stent-in-a-Tube Configuration

To simulate the oversizing when stent are implanted in vivo, the stents model was deployed in a silicone tube. According to the in vitro study of Nikanorov et al. (Ref 24), the tube was chosen with an internal diameter of 5.7 mm and a thickness of 3 mm, resulting in a tube-stent oversizing ratio of 1:1.4 ($D_{innertube}$: $D_{outerstent}$). A tube length of 100 mm was adopted; hence, the tube protrudes approximately of 27 mm at each stent sides. The silicone material was described as linear elastic material with the Young modulus E = 1.8 MPa and Poisson coefficient ν = 0.45 (Ref 29). The presence of the stent-tube oversizing requires the simulation of the stent crimping procedure within the tube and a subsequent step with the stent free to self-expand and to touch the tube inner wall. The adopted procedure and boundary conditions were previously described in Meoli et al. (Ref 20). Briefly, both phases are simulated by imposing a uniform radial displacement to a rigid cylindrical surface (initial diameter slightly bigger than the outer diameter of the stent) which is in contact with the stent outer surface. To apply the axial compression load to the stent model, the silicone tube was axially stretched by 5% before the stent deployment; then, after the device release, it was carried back to its original length and finally stretched again. A friction coefficient of 0.2 was defined for the stent-tube contact, as a result the device underwent cycles of axial shortening (Fig. 3b). Standard rigid-flexible contact pairs were created between the rigid body and the outer surface of the stent. No separation flexible-flexible contact pairs were defined between the outer surface of the stent and inner surface of the silicone tube. No separation involves that the contact surfaces are not allowed to separate, while they can slide over each other. This is consistent with reality since self-expanding stents due to stent-tube

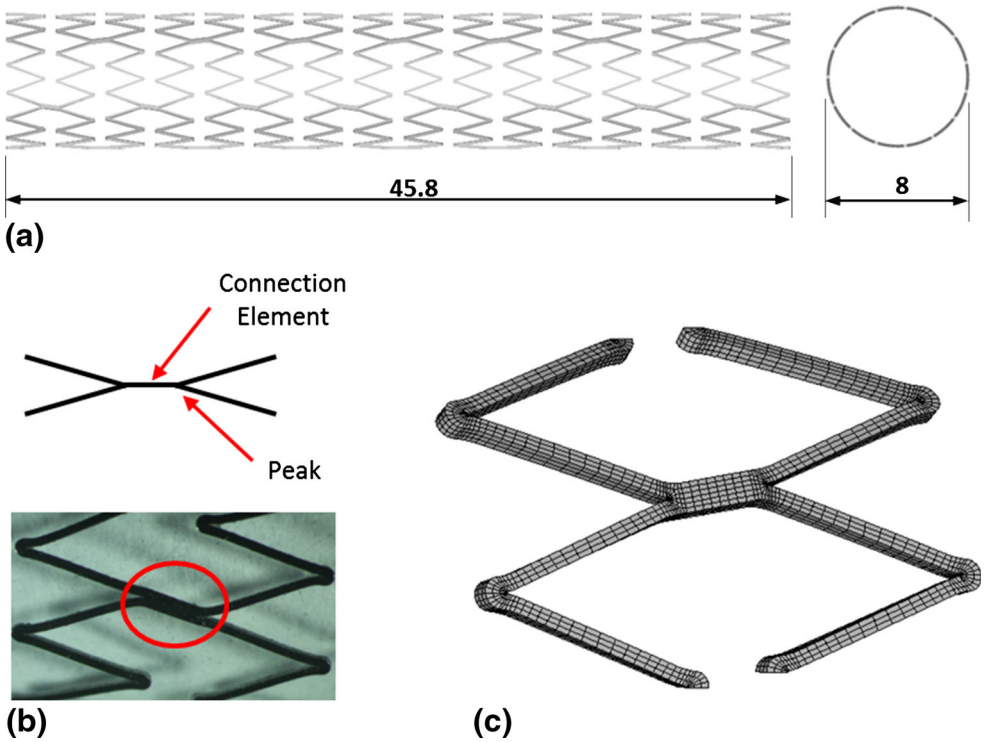

Fig. 1 In (a), geometric models of the Stent M. Dimensions reported are in mm. In (b), types of crown connection for the stent design. In (c), particular of the mesh S showing the higher density of elements nears the peaks

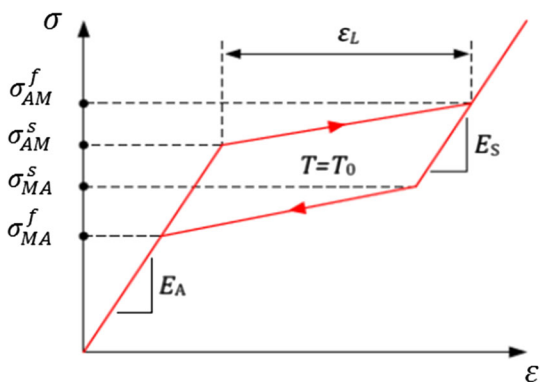

σ^f_{AM} (MPa)	442
σ^s_{AM} (MPa)	416
σ^f_{MA} (MPa)	104
σ^s_{MA} (MPa)	185
$E_A=E_M$ (MPa)	51100
ν	0.3
ε_L	0.04962
α	0.19

Fig. 2 On the left, the sketch of the uniaxial behavior of Nitinol material model is shown. σ^f_{AM} final stress value for the forward phase transformation (austenite A to martensite B); σ^s_{AM} starting stress value for the forward phase transformation; σ^f_{MA} final stress value for the reverse transformation (M to A); σ^s_{MA} starting stress value for the reverse transformation; ν Poisson's ratio; ε_L the maximum transformation strain reached at the end of the A to M transformation; $E_A = E_M$ austenite and martensite Young's modulus; α parameter accounting for the difference between material responses in tension and compression (for a uniaxial tension-compression test α can be related to the starting stress value for the A to M transformation in both tension (T) and compression (C) as $\alpha = \frac{\sigma^s_{AMC} - \sigma^s_{AMT}}{\sigma^s_{AMC} + \sigma^s_{AMT}}$)

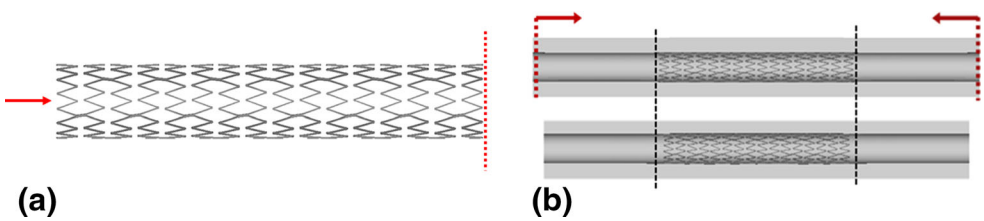

Fig. 3 Scheme of the structural simulations of axial compression for the Stent M in (a) the fully expanded configuration and (b) in the stent-in-a-tube configuration

oversizing exhibit a chronic radial force on the tube, which guarantees that stent remains in contact with the tube after stent deployment is performed.

2.4 Overlapping-Stents-in-a-Tube Configuration

To consider cyclic axial compression in case of overlapping stents, the subsequent deployment of two distinct models (length of 28.4 mm for each stent) with a zone of partial overlapping were simulated. Based on clinical studies (Ref 1, 5), the overlapping region was assumed to be 11 mm. Hence, after the stents deployment in the tube, the two stents cover a total length of 45.8 mm. Stent crimping and deployment were simulated following the procedure described above, using two rigid surfaces, one for each stent model, in a sequential manner; 5% of axial compression was applied stretching the tube before stents deployment. Standard rigid-flexible and no separation flexible-flexible contact pairs were defined for each stent model as for the stent-in-a-tube-configuration. A bonded flexible-flexible contact pairs were defined between the inner surface of the first deployed stent and the outer surface of the second deployed stent. Bonded contact implies that contact surfaces are not allowed to separate and they cannot slide over each other. This is based on the hypothesis that in real cases, some of the stent struts might interfere with each other. As a result, the relative movement of the two stents in the overlapping region is nearly zero. Thus, we assume a simplified interaction between the two stents that ensure faster solution time and easier convergence.

2.5 Risk of Fatigue Fracture

Nitinol fatigue fracture risk is assessed on the basis of amplitude and mean values of the cyclic principal strain in the stent (Ref 21-23). As proposed in recent studies, (Ref 21-23) to calculate mean (ε_m) and amplitude (ε_a) strain values in each stent element in response to the application of a load cycle, the following relations are used:

$$\varepsilon_m = \frac{(\varepsilon_{\max} + \varepsilon_{\min})}{2} \qquad \varepsilon_a = \left|\frac{(\varepsilon_{\max} - \varepsilon_{\min})}{2}\right|,$$

where max and min represent the highest and the lowest strain values in a loading cycle. For the two steps of the loading cycle, the maximum in absolute value between the first and third principal strain was identified at each element and stored with the proper sign obtaining $\varepsilon_{\max}$ and $\varepsilon_{\min}$. Then, the above relations were used to calculate ε_m and ε_a in each stent element. These quantities are examined both in the form of contour maps and as points coordinates plotted on a constant-life diagram.

3. Results

The contour maps reported in Fig. 4a show ε_m and ε_a for the Stent M in the case of fully expanded configuration. It can be noted that ε_m is equal to ε_a reaching a maximum value of 0.07%. Moreover, the strain distribution is repetitive through the stent length, and the highest values are located near the links in the internal portion of the strut peaks connected by a link. In case of stent-in-a-tube configuration, the mean strain differs from the amplitude strain both in terms of value and location of the highest strain zones (Fig. 4b). The mean strains reach a maximum value of 4.57% and are located for the entire stent in the external portion of the strut peaks not connected by a link. ε_a shows lower maximum values (0.17%) concentrated in the external portion of the strut peaks connected by a link.

Figure 5 shows the contour maps of ε_m and ε_a for the Stent M for the overlapping-stents-in-a-tube configuration. While no relevant difference in the maximum value of mean strain is observed with respect to the single stent case, a higher amplitude strain is reached (0.20%). The alternating strain field shows a non-uniform distribution, with higher strain values concentrated in the strut peaks connected by a link at the

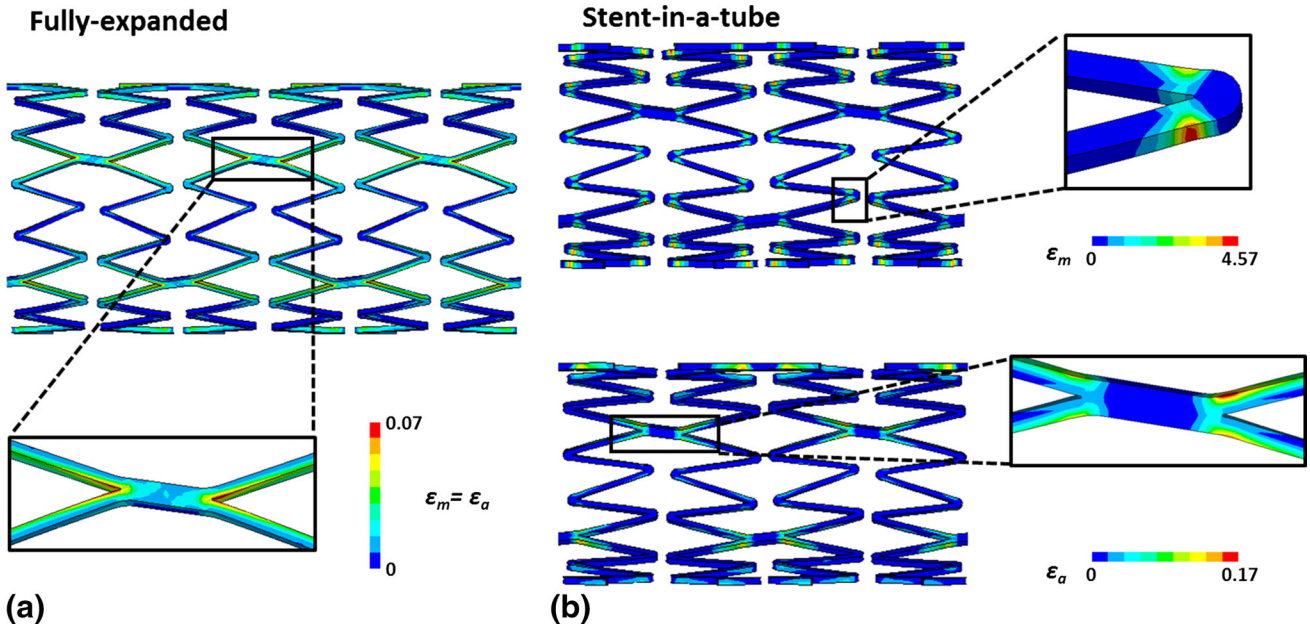

Fig. 4 Maximum principal mean (ε_m) and amplitude strain (ε_a) contours in the Stent M subjected to axial compression in the fully expanded (a) and stent-in-a-tube configurations (b)

interface between overlapping and single stent portions. Instead, in the overlapping region, the maximum ε_a calculated is 0.15%. At the stent sides, the maximum value of the amplitude strain is similar to the case of single stent deployed in a tube (0.17%).

Figure 6 reports the constant-life diagrams for the Stent M for cyclic axial compression for all the configurations. These diagrams confirmed the differences between the cases with and without the presence of a confining tube already highlighted by the strain distributions. Concerning the fully expanded configuration, all calculated data fall in the diagram area closest to the vertical axis. In particular, data lie on a line corresponding to the $\varepsilon_m = \varepsilon_a$ condition, coherently with the contour maps of Fig. 4a. In case of stent deployed in a tube (both single and double stent models), calculated data are distributed over a wider area in terms of mean strain components. Finally, the Stent M exhibits successively higher risk of fatigue fracture (i.e., higher ε_a) moving from fully expanded to single and double stent configurations.

It is worth noting that in the case of stent-in-a-tube and overlapping-stents-in-a-tube configurations due to material hysteresis and friction (stent-tube contact), three loading cycles have been simulated to achieve a stationary response in the stent. Concerning the fully expanded configuration, as a result of the applied zero-to-max-to-zero, only one cycle is required.

4. Discussion

In this work, the use of FEM coupled to fatigue analysis gave useful insights to investigate the fatigue behavior of a commercial Nitinol stent when subjected to cyclic axial compression in the expanded and deployed in tube (single and two overlapping stents) configurations. Current results confirmed for the Stent M the findings observed in a previous study for other stent designs (Ref 20); the fully expanded configuration produce very different fatigue response when compared to the case with stent deployed in a tube. The contour maps in Fig. 4a and b show a significant difference in both amplitude and mean strains induced in the stent. Strain distributions are different not only in terms of magnitude, but also in terms of locations of high strains, highlighting that the two loading configurations imply a completely different deformation modalities for the investigated device.

Regarding the overlapping-stents-in-a-tube model, overlapping does not cause relevant difference in terms of mean strains. Indeed, both magnitude and distribution of ε_m remain similar as in the case of a single stent. However, the amplitude strain shows higher values and different distributions (Fig. 5). The alternating strain field is no longer repetitive along the stents length, and higher values are concentrated in the peaks connected by a link and adjacent to the overlapping portion. In these regions, the transition from two overlapping stents to a single one causes a relevant change in the axial stiffness. Hence, the regions next to overlapping portion are subjected to higher axial shortening, while in the overlapping region a lower value of ε_a (0.15%) is reached due to a higher stiffness. This difference in the axial shortening is mainly due to the non-uniform slipping at the stent-tube interface caused by different stiffness of the overlapping portion. Moving toward the stent sides, ε_a has a value similar to that observed in the stent-in-a-tube configuration, suggesting that in this region the axial shortening is not affected by the overlapping. These observations help to explain the highest incidence of stent fracture observed in various clinical trials located at the margins of the overlapping portion in case of multiple stents implanted (Ref 7-9).

The different fatigue behaviors determined by the fully expanded configuration are also confirmed by the constant-life diagrams reported in Fig. 6. Calculated data fall on different

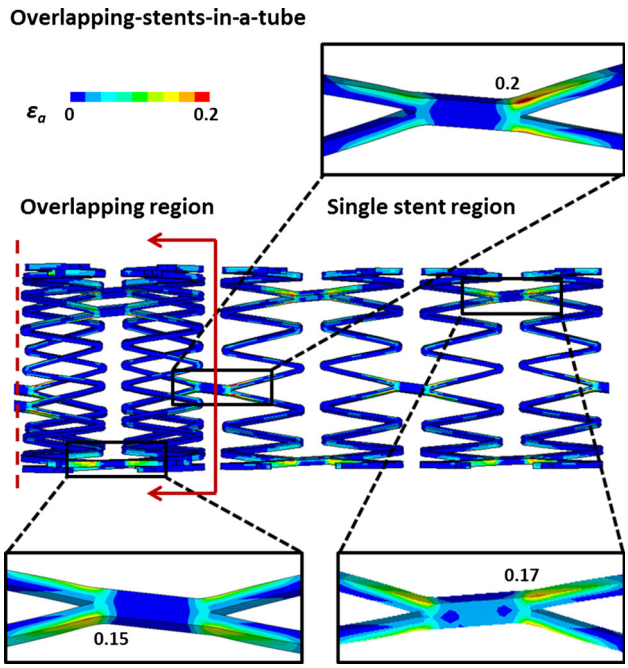

Fig. 5 Maximum principal amplitude strain (ε_a) contours in the Stent M when subjected to axial compression in the overlapping-stents-in-a-tube configuration. The red arrows indicate the beginning of the overlapping region. For clarity, only a part of the model is shown. The dotted line indicates the middle axis of the model

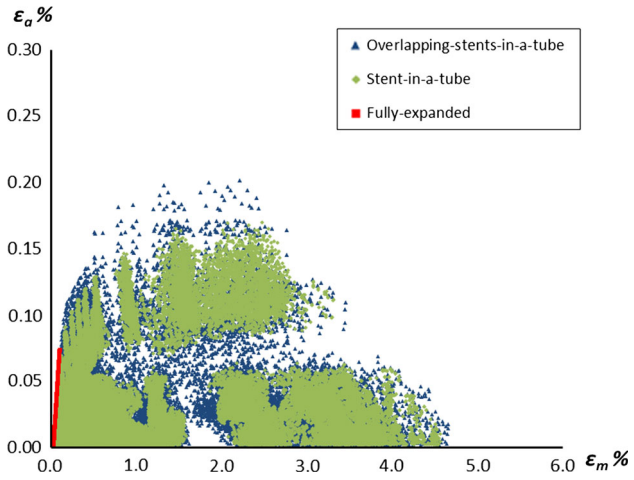

Fig. 6 Constant-life diagram for axial compression of Stent M in the fully expanded, stent-in-a-tube, and overlapping-stent-in-a-tube configurations

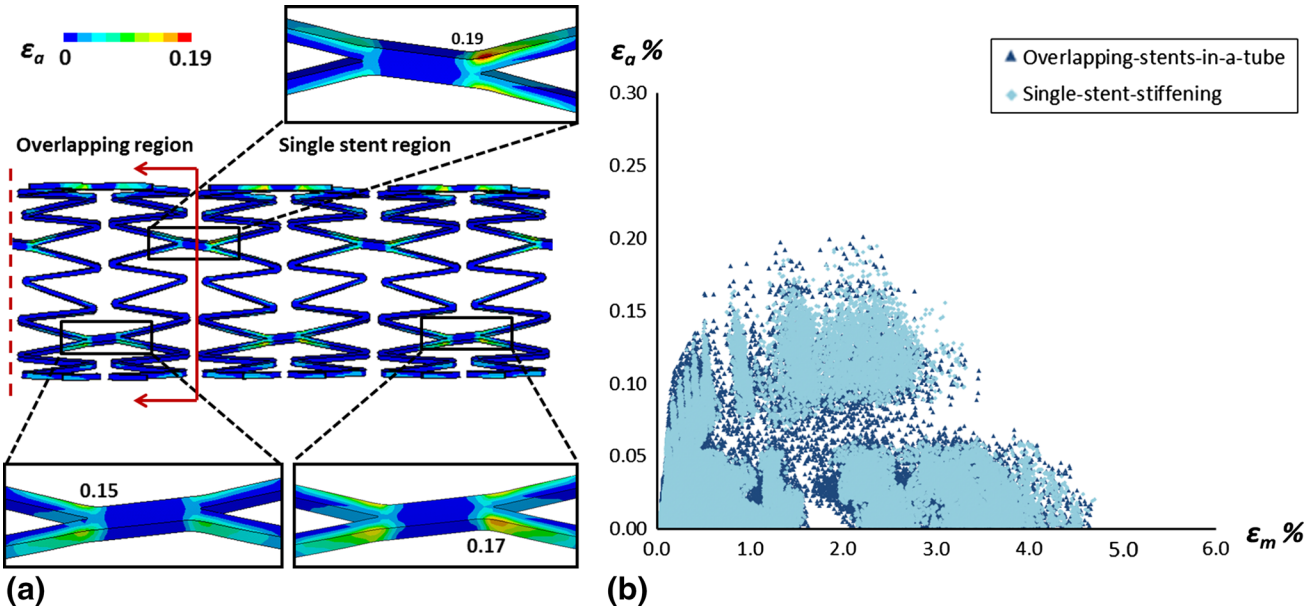

Fig. 7 In (a) maximum principal amplitude strain (ε_a) contours in the Stent M when subjected to axial compression in case of stent-in-a-tube configuration with higher stiffness in the central four strut crowns. The red arrows indicate begin of the overlapping region. For clarity, only a part of the model is shown. The dotted line indicates the middle axis of the model. In (b), constant-life diagram for axial compression of Stent M in stent-in-a-tube and overlapping-stents-in-a-tube configurations

areas of the diagrams. For the fully expanded configuration, ε_m and ε_a are equal in magnitude, while for the stent-in-a-tube and overlapping-stents-in-a-tube configurations, the mean strain is always higher than the alternating strain. The trends of ε_m and ε_a in fully expanded configuration are as a result of the applied zero-to-max-to-zero loading condition. Regarding the configurations in which the stents are released in a silicon tube, as the devices cannot recover their nominal diameter because of the stent-wall interaction represented by to the stent-tube oversizing, a higher mean deformation component is induced. The calculated data are distributed over a wider diagram area in terms of ε_m and stent rupture may occur for a wide range of mean strain depending on the specific fatigue limit curve, which is unknown for the stent material considered in this study.

Concerning the amplitude strain, it is worth noting that in case of stent deployed in a tube, the cyclic shortening applied to the stent is lower than in the case of fully expanded configuration (4.7 versus 5%). This is due to the fact that the 5% shortening applied to the tube was not completely transferred to the device. This might be related in part to a little sliding between the stent and the tube and in part to the fact that the region where stent is deployed has a higher axial stiffness compared to the parts where only the tube is present. Hence, the two sides of the tube, where the stent is absent, accommodate more deformation than the central part where the stent contributes to increase the axial stiffness of the system. Even if the shortening imposed to the stent models is less in case of stent-in-a-tube configuration, our simulations indicate that the oversizing has an influence also on the maximum value reached in the stent. Indeed, in case of stent deployed in a tube, the maximum value of ε_a is more than double (0.07 versus 0.17). These results are consistent with a previous computational work where the fully expanded and stent-in-a-tube configurations were investigated for different stent designs (Ref 20). The current results confirm the importance of oversizing in determining the fatigue behavior of peripheral Nitinol stents and show that the influence of stent oversizing on ε_a is stent design dependent. Experimental studies on animal models (Ref 30, 31) showed that even though after implantation Nitinol stents were constrained by their target artery diameter, they expanded approximately to their nominal diameter within 6 months. This implies that devices are progressively loaded with a decreasing oversizing ratio until the nominal diameter is totally recovered. However, according to a typical Wohler diagram for Nitinol (Ref 23), the fatigue limit at 10^5 cycles is very similar to the endurance of material. Since 1 year of walking represent 1 million of loading cycles for devices implanted in the SFA, the in vivo conditions in the first months after stent deployment, when the stent oversizing is higher, are crucial. Moreover, Lownie et al. (Ref 32) observed minimal late expansion in case of calcified plaque in a clinical study on human carotid arteries. This can be explained with a higher stiffness associated with calcified lesions that prevents the delayed expansion of the devices. Since lesions in the SFA are often long and diffuse with high calcification degrees (Ref 6, 10, 33, 34), it can be speculated that peripheral stents maintain a certain oversizing over time. Based on the evidence above, we suggest that the presence of the oversizing cannot be disregarded when investigating the fatigue performance of Nitinol stents.

The comparison on the constant-life diagram (Fig. 6) of the stent-in-a-tube and overlapping-stents-in-a-tube, as expected, shows that the overlapping condition is associated with a higher risk of fatigue failure. Indeed, for equal mean strains, the amplitude strain is higher (0.17 versus 0.2%). It is worth noting that in the overlapping-stents-in-a-tube model, all the amplitude strain data with values higher than 0.17% (maximum ε_a for the single stent model) are located in the portion next to the overlapping region.

To investigate more in detail the effects of increasing axial stiffness due to the overlapping of multiple stents, we carried out an additional simulation on a simplified model. Assuming

that the overlapping portion of the stents has twice the stiffness of a single one (Ref 18), only a device was considered with a whole length of 45.8 mm with a central region of 11 mm (four strut crowns) in which the material properties were changed doubling the stiffness of the material. The resulting condition is representative of the release of two stents each with a length of about 28.4 mm, overlapping for a length of 11 mm. Axial compression of 5% has been applied following the procedure described for the stent-in-a-tube configuration.

Results show that amplitude strain distribution through the stent (Fig. 7a) is very similar to that obtained for the overlapping-stents-in-a-tube model. Higher strains are concentrated in the peaks connected by link near the overlapping region, while the central portion is subjected to lower cyclic compression. The comparison on the constant-life diagram (Fig. 7b) shows very similar results for the two considered models confirming the higher risk of fracture associated with this condition and supporting the hypothesis that discontinuity in the axial stiffness has a role in determining higher rates of stent fracture.

5. Conclusions

In this study, simulations of axial compression for a peripheral Nitinol stent were performed, allowing the investigation of fatigue behavior of peripheral Nitinol stents taking into account important aspects of the loading conditions the devices are subjected to during their in vivo functioning. Our findings confirm the importance of the stent oversizing in determining the fatigue performance in the femoropopliteal region. Indeed, the stent-wall interaction plays an important role in determining both mean and amplitude strains induced in the stents subjected to axial compression. Moreover, our results help explain the high incidence of stent fracture located close to the overlapping portion observed in various clinical trials. Higher risk of fatigue failure is associated to overlapping-stents. The single stent model with stiffening of the central region to simulate the presence of overlapping stents showed interesting results confirming that discontinuity in the axial stiffness could represent the cause of higher fracture risk in the portion next to the overlapping zone. Finally, a lower stent axial shortening in case of stents deployed in tube due to sides' effect, highlighted the need of standardized procedures for bench testing. In these regards, computational simulations could represent a useful tool to help researchers in defining in vitro set-up for evaluation of fatigue performance of Nitinol stents used in the SFA.

Acknowledgments

This work is within the project "RT3S - Real Time Simulation for Safe vascular Stenting" partially funded by the European Commission under the 7th Framework Programme, GA FP7-2009-ICT-4-248801.

References

1. P. Dick, H. Wallner, S. Sabeti, C. Loewe, W. Mlekusch, J. Lammer, R. Koppensteiner, E. Minar, and M. Schillinger, Balloon Angioplasty Versus Stenting with Nitinol Stents in Intermediate Length Superficial Femoral Artery Lesions, *Catheter. Cardiovasc. Interv.*, 2009, **74**, p 1090–1095
2. J.M. Gibbs, S.P. Costantino, and J. Benenati, Treating the Diseased Superficial Femoral Artery, *Tech. Vasc. Interv. Radiol.*, 2010, **13**, p 37–42
3. H. Krankenberg, M. Schlüter, H. Steinkamp, K. Bürgelin, D. Scheinert, K.L. Schulte, E. Minar, P. Peeters, M. Bosiers, G. Tepe, B. Reimers, F. Mahler, T. Tübler, and T. Zeller, Nitinol Stent Implantation Versus Percutaneous Transluminal Angioplasty in Superficial Femoral Artery Lesions up to 10 cm in Length: The Femoral Artery Stenting Trial (FAST), *Circulation*, 2007, **116**(3), p 285–292
4. J.R. Laird, B.T. Katzen, D. Scheinert, J. Lammer, J. Carpenter, M. Buchbinder, R. Dave, G. Ansel, A. Lansky, E. Cristea, T.J. Collins, J. Goldstein, and M.R. Jaff, Nitinol Stent Implantation Versus Balloon Angioplasty for Lesions in the Superficial Femoral Artery and Proximal Popliteal Artery. Twelve-Month Results from the RESILIENT Randomized Trial, *Circ. Cardiovasc. Interv.*, 2010, **3**(3), p 267–276
5. M.W. Mewissen, Primary Nitinol Stenting for Femoropopliteal Disease, *J. Endovasc. Ther.*, 2009, **16**(2), p 1163–1181
6. M. Schillinger, S. Sabeti, P. Dick, J. Amighi, W. Mlekusch, O. Schlager, C. Loewe, M. Cejna, J. Lammer, and E. Minar, Sustained Benefit at 2 Years of Primary Femoropopliteal Stenting Compared with Balloon Angioplasty with Optional Stenting, *Circulation*, 2007, **115**, p 2745–2749
7. D.E. Allie, C.J. Hebert, and C.M. Walker, Nitinol Stent Fracture in the SFA, *Endovasc. Today*, 2004, **8**, p 22–34
8. D. Scheinert, S. Scheinert, J. Sax, C. Piorkowski, S. Braunlich, M. Ulrich, G. Biamino, and A. Schmidt, Prevalence and Clinical Impact of Stent Fractures After Femoropopliteal Stenting, *J. Am. Coll. Cardiol.*, 2005, **45**(2), p 312–315
9. S.H. Duda, M. Bosiers, J. Lammer, D. Scheinert, T. Zeller, V. Oliva, A. Tielbeek, J. Anderson, B. Wiesinger, G. Tepe, A. Lansky, M.R. Jaff, C. Mudde, H. Tielemans, and J.P. Beregi, Drug-Eluting and Bare Nitinol Stents for the Treatment of Atherosclerotic Lesions in the Superficial Femoral Artery: Long-Term Results from the SIROCCO Trial, *J. Endovasc. Ther.*, 2006, **13**(6), p 701–710
10. M. Bosiers, G. Torsello, H.M. Gissler, J. Ruef, S. Müller-Hülsbeck, T. Jahnke, P. Peeters, K. Daenens, J. Lammer, H. Schroë, K. Mathias, R. Koppensteiner, F. Vermassen, and D. Scheinert, Nitinol Stent Implantation in Long Superficial Femoral Artery Lesions: 12-Month Results of the DURABILITY I, Study, *J. Endovasc. Ther.*, 2009, **16**(3), p 261–269
11. O. Iida, M. Uematsu, Y. Soga, K. Hirano, K. Suzuki, H. Yokoi, T. Muramatsu, N. Inoue, S. Nanto, and S. Nagata, Timing of the Restenosis Following Nitinol Stenting in the Superficial Femoral Artery and the Factors Associated with Early and Late Restenosis, *Catheter Cardiovasc. Interv.*, 2011, **78**(4), p 611–617
12. K.L. Schulte, S. Müller-Hülsbeck, P. Cao, J.P. Becquemin, R. Langhoff, P. Desgranges, H. Kobeiter, M. Midulla, V. Vladimir Borovicanin, D. Paunovic, and J.P. Beregi, MISAGO 1: First-In Man Clinical Trial with Misago Nitinol Stent, *EuroIntervention*, 2010, **5**, p 687–691
13. N. Bessias, G. Sfyroeras, and K.G. Moulakakis, Renal Artery Thrombosis Caused by Stent Fracture in a Single Kidney Patient, *J. Endovasc. Ther.*, 2005, **12**, p 516–520
14. S. Sahin, A. Memis, M. Parildar, and I. Oran, Fracture of a Renal Artery Stent due to Mobile Kidney, *Cardiovasc. Intervent. Radiol.*, 2005, **28**, p 683–685
15. H.B Lim, G. Hur, S.Y. Kim, Y.H. Kim, S.U. Kwon, W.R. Lee, and S.J. Cha, Coronary stent fracture: Detection with 64-Section Multidetector CT Angiography in Patients and In Vitro, *Radiology*, 2008, **249**, p 810–819
16. H.M. Hsiao, S. Prabhu, A. Nikanorov, and M. Razavi, Respiration Induced Kidney Motion on Cobalt-Chromium Stent Fatigue Resistance, *J. Biomed. Mater. Res. B*, 2009, **91B**(2), p 508–516
17. K.K. Kapnisis, D.O. Halwani, B.C. Brott, P.G. Anderson, J.E. Lemons, and A.S. Anayiotos, Stent Overlapping and Geometric Curvature Influence the Structural Integrity and Surface Characteristics of Coronary Nitinol Stents, *J. Mech. Behav. Biomed.*, 2013, **20**, p 227–236
18. B. Smouse, A. Nikanorov, and D. La Flash, Biomechanical Forces in the Femoropopliteal Arterial Segment, *Endovasc. Today*, 2005, **4**(6), p 60–66
19. L. Petrini, W. Wu, E. Dordoni, A. Meoli, F. Migliavacca, and G. Pennati, Fatigue Behavior Characterization of Nitinol for Peripheral Stents, *Funct. Mater. Lett.*, 2012, **5**(1), p 1–4

20. A. Meoli, E. Dordoni, L. Petrini, F. Migliavacca, G. Dubini, and G. Pennati, Computational Modelling of In Vitro Set-Ups for Peripheral Self-Expanding Nitinol Stents: The Importance of Stent-Wall Interaction in the Assessment of the Fatigue Resistance, *Cardiovasc. Eng. Tech.*, 2013, **4**(4), p 474–484
21. S.M. Harvey, Nitinol Stent Fatigue in Peripheral Artery Subjected to Pulsatile and Articulation Loading, *J. Mater. Eng. Perform.*, 2011, **20**(4-5), p 697–705
22. C. Kleinstreuer, Z. Li, C.A. Basciano, S. Seelecke, and M.A. Farber, Computational Mechanics of Nitinol Stent Grafts, *J. Biomech.*, 2008, **41**, p 2370–2378
23. A.R. Pelton, V. Schroeder, M.R. Mitchell, X.Y. Gong, M. Barney, and S.W. Robertson, Fatigue and Durability of Nitinol Stents, *J. Mech. Behav. Biomed. Mater.*, 2008, **1**, p 153–164
24. A. Nikanorov, H.B. Smouse, K. Osman, M. Bialas, S. Shrivastava, and L.B. Schwartz, Fracture of Self-Expanding Nitinol Stents Stressed In Vitro Under Simulated Intravascular Conditions, *J. Vasc. Surg.*, 2008, **48**(2), p 435–440
25. C.P. Cheng, N.M. Wilson, R.L. Hallett, R.J. Herfkens, and C.A. Taylor, In Vivo MR Angiographic Quantification of Axial and Twisting Deformations of the Superficial Femoral Artery Resulting from Maximum Hip and Knee Flexion, *J. Vasc. Interv. Radiol.*, 2006, **17**(6), p 979–987
26. A.J. Klein, S.J. Chen, J.C. Messenger, A.R. Hansgen, M.E. Plomondon, J.D. Carroll, and I.P. Casserly, Quantitative Assessment of the Conformational Change in the Femoropopliteal Artery with the Leg Movement, *Catheter Cardiovasc. Interv.*, 2009, **74**(5), p 787–798
27. A. Ganguly, J. Simons, A. Schneider, B. Keck, N.R. Bennett, R.J. Herfkens, and R. Fahrig, In-Vivo Imaging of Femoral Artery Nitinol Stents for Deformation Analysis, *J. Vasc. Interv. Radiol.*, 2011, **22**(2), p 244–249
28. S. Müller-Hülsbeck, P.J. Schäfer, N. Charalambous, H. Yagi, M. Heller, and T. Jahnke, Comparison of Second-Generation Stents for Application in the Superficial Femoral Artery: An In Vitro Evaluation Focusing on Stent Design, *J. Endovasc. Ther.*, 2010, **17**(6), p 767–776
29. F. Schneider, T. Fellner, J. Wilde, and U. Wallrabe, Mechanical Properties of Silicones for MEMS, *J. Micromech. Microeng.*, 2008, **18**(6), p 1–9
30. A.M. Saguner, T. Traupe, L. Raber, N. Hess, Y. Banz, A.R. Saguner, N. Diehm, and O.M. Hess, Oversizing and Restenosis with Self-Expanding Stents in Iliofemoral Arteries, *Cardiovasc. Interv. Radiol.*, 2012, **35**(4), p 906–913
31. H.Q. Zhao, A. Nikanorov, R. Virmani, R. Jones, E. Pacheco, and L.B. Schwartz, Late Stent Expansion and Neointimal Proliferation of Oversized Nitinol Stents in Peripheral Arteries, *Cardiovasc. Interv. Radiol.*, 2009, **32**(4), p 720–726
32. S.P. Lownie, D.M. Pelz, D.H. Lee, S. Men, I. Gulka, and P. Kalapos, Efficacy of Treatment of Severe Carotid Bifurcation Stenosis by Using Self-Expanding Stents Without Deliberate Use of Angioplasty Balloons, *Am. J. Neuroradiol.*, 2005, **26**(5), p 1241–1248
33. Z.M. Arthurs, P.D. Bishop, L.E. Feiten, M.J. Eagleton, D.G. Clair, and V.S. Kashyap, Evaluation of Peripheral Atherosclerosis: A Comparative Analysis of Angiography and Intravascular Ultrasound Imaging, *J. Vasc. Surg.*, 2010, **51**(4), p 933–938
34. T. Zeller, Current State of Endovascular Treatment of Femoro-Popliteal Artery Disease, *Vasc. Med.*, 2007, **12**(3), p 223–234